J. Fluid Mech. (1982), *vol.* 122, *pp.* 195–213
Printed in Great Britain

Experiments on leapfrogging internal solitary waves

By P. D. WEIDMAN† AND M. JOHNSON
Department of Aerospace Engineering, University of Southern California, Los Angeles, California 90007

(Received 9 March 1981 and in revised form 2 March 1982)

Experiments on the resonant energy transfer between internal gravity-wave solitons travelling along neighbouring pycnoclines have been performed. Measurements of both amplitude and phase oscillations are found to be in qualitative agreement with theoretical predictions given in the companion paper by Liu, Pereira & Ko (1982). Using averaged quantities to account approximately for wave-energy dissipation, the theoretical expression correlating the oscillation frequency with the density environment parameters is reasonably well verified. A new three-soliton resonance requiring both upstream and downstream energy transfer has also been observed.

1. Introduction

The strong interaction between two Korteweg–de Vries (KdV) solitary waves travelling unidirectionally along a single density interface is now well understood. Of the three types of collisions cited by Lax (1968), the type (*a*) interaction between waves travelling at nearly the same phase speed is perhaps the most interesting. In this case the larger amplitude wave approaches but does not override the lead wave. Instead, the two peaks remain distinct throughout the interaction while the waves exchange amplitudes during the time they propagate in close proximity to one another. Once the energy transfer is complete, the larger-amplitude lead wave propagates permanently away from the rear wave owing to its enhanced wave speed, and the only remnant of the collision is a small permanent phase shift incurred by each soliton. This energy exchange between two mode-one (single-hump) waves of elevation with initial speeds $C_1 > C_2$ is illustrated in figure 1. All three types of interactions discussed by Lax (1968) have been documented by Weidman & Maxworthy (1978) in their free-surface wave experiments, and similar interactions are easily demonstrated in the laboratory for mode-two (bulge) internal waves travelling along a single pycnocline in a density-stratified fluid. A characteristic feature of such interactions is the forward or *upstream* transfer of energy from the initially larger trailing soliton to the smaller lead soliton.

Let us consider now an interaction wherein two mode-two internal solitary waves move unidirectionally, but along vertically separated pycnoclines as depicted in figure 2, again with a relatively small difference in their phase speeds. Intuition suggests what would happen in the limiting cases of very small or large separation between the density interfaces. In the latter case the two solitary waves would propagate

† Present address: Department of Mechanical Engineering, University of Colorado, Boulder, Colorado 80309.

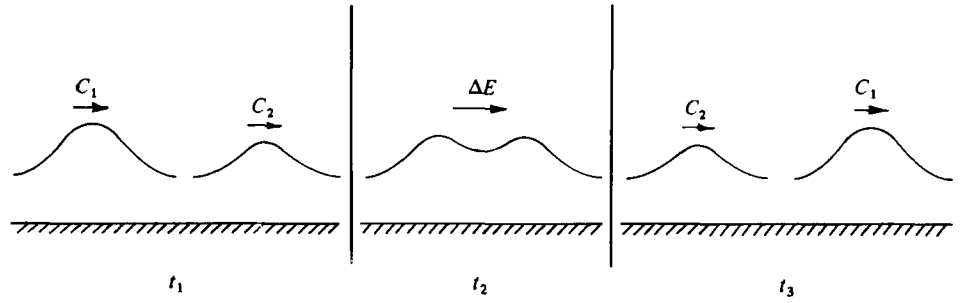

FIGURE 1. Sketch illustrating the *upstream* energy transfer between free-surface solitons travelling from left to right during a type (*a*) interaction described by Lax (1968). The times t_1, t_2, and t_3 are successive instants before, at the middle of, and after the interaction respectively.

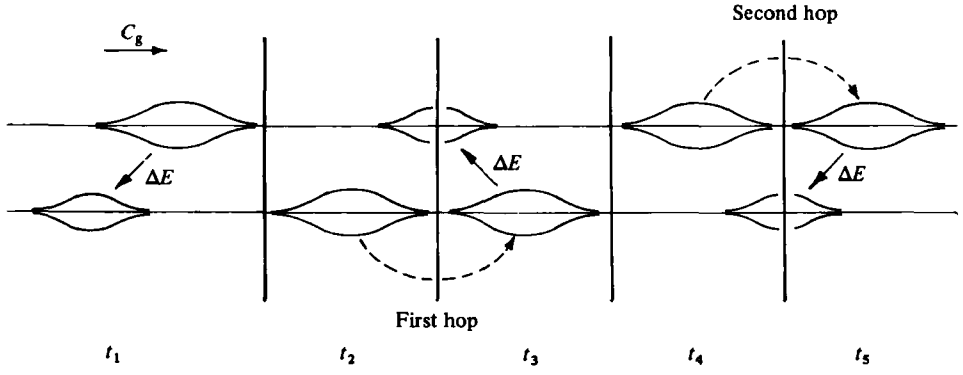

FIGURE 2. Sketch illustrating the *downstream* energy transfer between mode-two internal-wave solitons travelling along neighbouring pycnoclines. The wave system is moving from left to right at the group velocity. The times $t_1, \ldots, t_5$ denote successive times during the resonant cycle.

independently, the faster overtaking the slower without energy exchange; in the former case the two interfacial regions would overlap, forming essentially a single pycnocline, and the interaction would be characterized by a single upstream energy transfer from the lagging to the leading disturbance. In the intermediate case, where the pycnoclines are distinctly separated but not too far apart, a new phenomenon is possible: energy can be transferred rearward or *downstream* from the larger, temporarily leading wave to the smaller, temporarily lagging one on the neighbouring pycnocline. Then, in a reference frame following the mean velocity of the system, the two waves will exchange their horizontal positions owing to the growth and relatively greater speed of the trailing soliton as illustrated in figure 2. Under such 'resonance' conditions in an ideal fluid, energy will be exchanged alternately between solitary waves in the downstream direction, and successive upstream hops will ensue in leapfrog fashion.

The present experiment to investigate this novel feature was motivated by the nonlinear analysis of Liu, Kubota & Ko (1980) (hereinafter referred to as LKK), although studies of resonant interactions for linear internal waves date back to Eckart (1961). Denoting a typical soliton wavelength by λ and the separation between pycnoclines by H, the investigation in LKK dealt with pycnocline separations for which $H/\lambda = O(1)$; the numerical integrations of the governing pair of coupled evolution equations for this parameter regime clearly exhibit the resonant energy transfer

described above. In the companion paper to this study Liu, Pereira & Ko (1982) (hereinafter referred to as LPK) have considered the case of weak coupling that occurs when $H/\lambda \gg O(1)$. Similar leapfrog oscillations are predicted, and explicit asymptotic formulae are derived relating the leapfrog oscillation frequency to the ambient-density-field parameters and wave amplitudes for the special case of Joseph (1977) solitons.

A description of the experimental facility and measurement techniques is given in § 2. In § 3 we present and discuss the measured results, including an observation of a three-soliton interaction, and concluding remarks are relegated to § 4.

2. Apparatus and data acquisition

Our experimental facility, the important features of which are sketched in figure 3, consisted of a wave-generation unit followed by 10 m of rectangular Lucite channel 20 cm wide by 30 cm deep. The channel was levelled to about $\pm 1{\cdot}5$ mm over its entire length with the aid of adjustable screws supporting the working sections.

For all experiments reported here, the ambient stratification consisted of three uniform layers of saline water separated by two pycnoclines at the one-quarter and three-quarter fluid-depth levels. The density variation through each layer closely resembled a hyperbolic-tangent density profile. In each case the total depth was very nearly 30 cm, with densities $\rho = 1{\cdot}02$, $1{\cdot}05$, and $1{\cdot}08$ g/cm^3 in the upper, middle and lower layers respectively. The mixing of the different fluids at their interfaces during the filling process was minimized by slowly metering the fluid for each new layer through porous floating rafts. The lower pycnocline was on the average 11 % thicker than the upper one owing to diffusion during the two hours that elapsed before the formation of the upper pycnocline.

After considering several wave-generation methods, it was determined that nearly identical mode-two waves could best be initiated by the simple collapse of two separately mixed regions. (Detailed studies of waves formed in this manner can be found in Amen & Maxworthy 1980; Maxworthy 1980.) In figure 3 we see that the wave generator consisted of two mixing chambers separated by a horizontal splitter plate $1{\cdot}25$ cm thick located at mid-depth and extending some 40 cm beyond the end of a removable barrier. A top plate of the same length wetted the upper surface to inhibit the production of free-surface waves during barrier removal, and to ensure a symmetric collapse of the upper and lower mixed-regions. The rear walls of the mixing chambers were sealed around their perimeter with porous weather-stripping so that they could be positioned *in situ* fore and aftto provide a range of initial mixed volumes. Also shown in figure 3 are the mixing propellers with shafts sealed at, and extending through, the rear wall for exterior drive using a variable-speed motor.

2.1. *Description of wave generation and interaction*

After some experimentation we found that leapfrog interactions were readily obtained with nearly identical initial conditions (i.e. equal chamber volumes and mixedness, and nearly equal pycnocline thicknesses) and rapid barrier removal so that the gravitational collapse of each region began almost simultaneously. Under these conditions the two lead solitons were observed to initially travel in unison: both collapsed regions formed nearly identical lead waves with similar dispersive tails; after

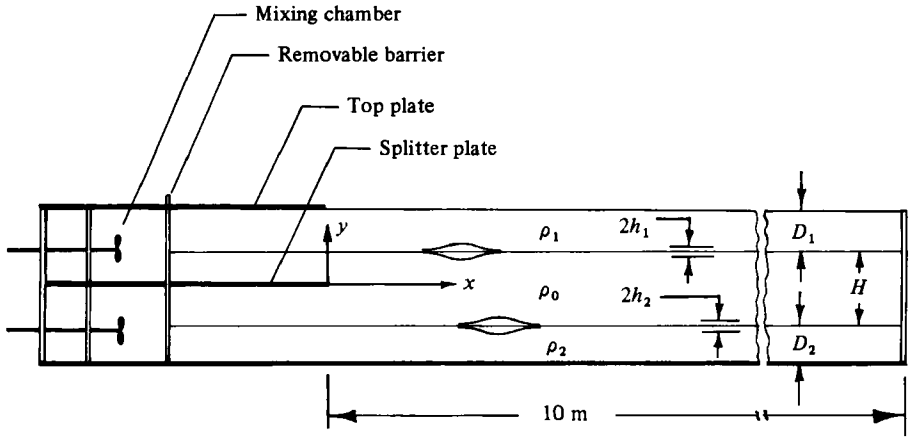

FIGURE 3. Sketch of the experimental tank and wave generator.

leaving the splitter plate the solitons continued to travel together (presumably because of a symmetric interaction between the wave systems), each vying for the lead position. The lower wave generally pulled ahead first because, owing to the greater thickness of the lower pycnocline, it had a slightly larger linear long-wave phase speed for the otherwise equal density jumps and symmetric location of the pycnoclines about mid-depth (see (3.6)). Once in the lead, it began to transmit energy backwards to the upper wave, which grew and subsequently initiated the first hop. Although the solitons diminished in amplitude significantly during their flight down the 10 m tank, the leapfrog oscillations continued unabated since the effects of dissipation acted equally on each wave and preserved the crucial small difference between their phase speeds.

Coloured dye mixed uniformly with the fluid in each chamber allowed the following observations. The gravitational collapse formed gravity currents which evolved into mode-two solitary waves carrying mass from the original mixed volume in the form of embedded counter-rotating fluid cells. Such waves characterized by internal recirculating flow were observed only at large amplitudes, and hence are labelled *strong* solitons. The viscous self-erosion of the cells continually deposited the transported fluid in a thin sheet behind the propagating waves. All traces of recirculation disappeared before or at the end of the first complete hop; from this point onward the waves lacked closed streamlines and are labelled *weak* solitons. (Similar observations of the formation of a *strong* soliton from the collapse of a single mixed-region and its evolution into a *weak* soliton are reported by Maxworthy (1980).)

Large-amplitude waves were generated in most cases to ensure good wave crest and amplitude definition for the two or three complete hops that transpired before the waves reached the end of the test facility. Including the return path from the end wall back to the wave generator, as many as five complete hops were observed, but the returning wave crests were often too small and flat to be accurately followed and recorded.

We note that the presence of the top plate in contact with the free surface did in fact inhibit the formation of surface gravity waves. However, a slow free-surface drift just above the upper solitary wave was evident, clearly a manifestation of mass conservation in the stratified fluid system.

2.2. *Measurement techniques*

The waves were visualized with the aid of neutrally buoyant tracer droplets composed of a kerosene–Freon mixture coloured with red dye and located at preselected levels above and below the centre of each pycnocline. Droplet-size control and prevention of density deterioration (through the rapid evaporation of the more volatile Freon) were attained by pressurizing the mixture in a closed reservoir and ejecting it through a rake of twelve small hypodermic tubes immersed just below the free surface and spanning the breadth of the channel. The droplets ranged from 0·5 to 3 mm in diameter, and, after falling to their predetermined depth, gave the appearance of a carpet of red beads.

Ambient density profiles were measured with conductivity probes and associated electronics. The sensor consisted of a platinum coated metallic cathode bead (about 0·15 mm diameter) fixed at the drawn tip of a long slender glass cylinder. The cylinder enclosed a wire filament that conducted the signal to an output connector at the opposite end, and a 2·4 mm stainless-steel rod served as the anode. Both cathode and anode elements were mounted parallel to one another (about 1 cm apart) on a vertical traversing mechanism. This arrangement was devised in an attempt to provide nearly identical conducting paths through the fluid in both the measurement and calibration environments. A practical discussion of the operation of these probes and their inherent problems is given by Koop (1976).

The conductivity probe was used initially to trace out the uncalibrated density distribution through each pycnocline in order to locate approximately the kerosene–Freon beads just inside the 'corners' of each hyperbolic-tangent profile. Also, either before or after each experiment, a vertical density profile and calibration with 7 or 8 accurately measured reference densities was taken for each layer separately. This separate recording of the two pycnocline profiles was necessary to maintain reasonable measurement accuracy ($d\rho/\rho = \pm 0{\cdot}0015$) owing to the extreme nonlinearity of the density–voltage curve at low densities.

Amplitude and trajectory data were obtained photographically. A permanent grid (1·0 cm vertical × 2·0 cm horizontal) marked with waterproof ink on the inside wall of the channel provided a fixed reference frame. Two Nikon cameras were mounted on a trolley in a vertical plane, one at each pycnocline level. As the trolley was pushed alongside the channel to follow the interacting waves, relays fired by a pulse from a function generator simultaneously triggered the two cameras, and time intervals between successive photographs were measured with a Hewlett–Packard timer–counter. The double-camera system was devised to eliminate errors in amplitude measurement due to parallax.

Wave trajectories were obtained from enlarged projections of the negatives by measuring the wave-crest position at each time interval. The wave amplitudes, defined as one-half the difference between the maximum droplet separation produced by a passing wave and the undisturbed droplet separation, were also recorded. Tests showed that amplitudes obtained from droplets located 5 % of the maximum slope thickness above or below their nominal positions yielded little measurable difference. It was concluded, therefore, that the tracer droplets must have been positioned near the extrema of the spatial eigenfunction for each mode-two wave, and hence the data reported here are indicative of the maximum wave amplitudes. Measurement errors

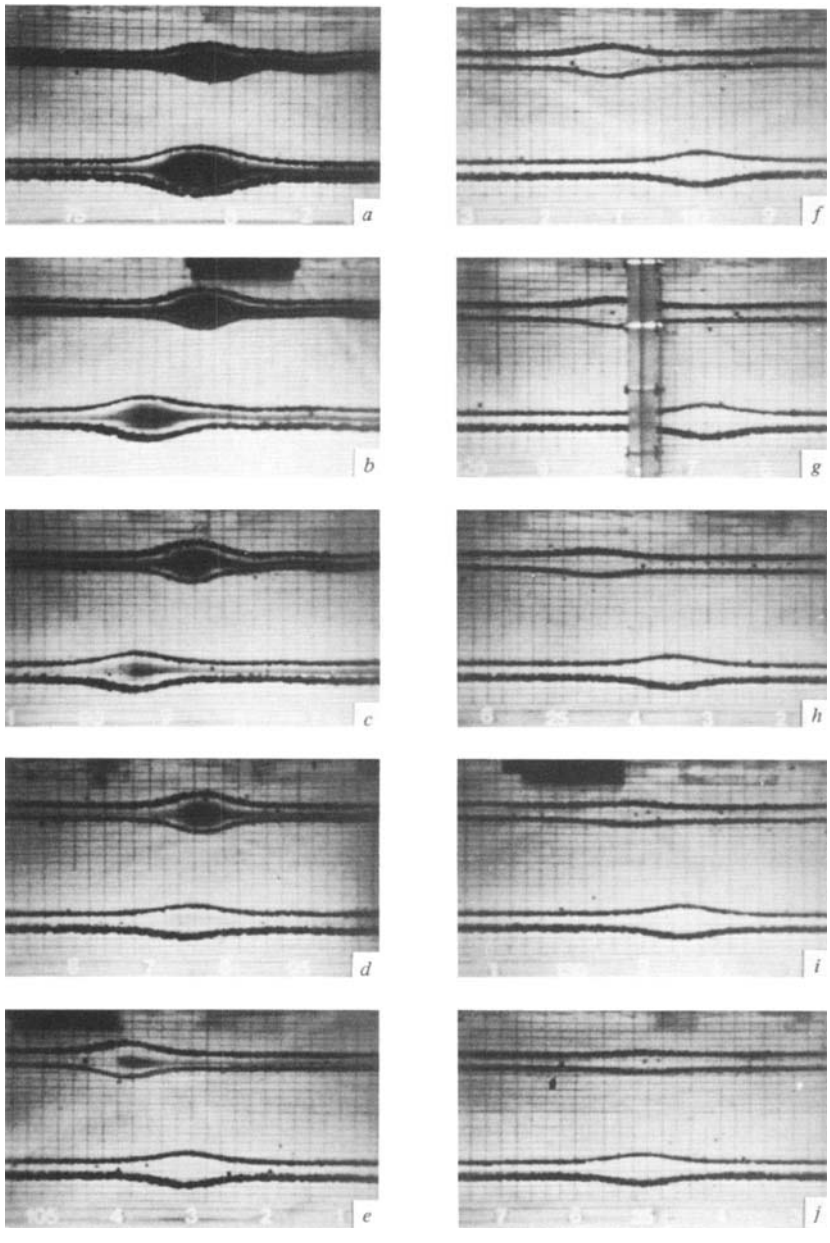

FIGURE 4. Photographic sequence exhibiting a solitary-wave resonant interaction over one complete cycle of oscillation taken from a ciné film strip. The waves propagate from right to left, and time increases from (*a*) to (*j*) with a constant time interval of 20 s between frames. The numbers at the bottom of each photograph represent the relative downstream position in dm.

in the position of the wave crests depend on the sharpness of the peaks, and ranged from approximately ± 2 to ± 6 mm. Absolute amplitude-measurement errors are estimated to be $\pm 0{\cdot}75$ mm, although the relative error for measurements in a given experiment may be considerably less.

The qualitative features of a typical interaction can be seen in figure 4, which com-

prises a sequence of photographs taken from a single film strip over one complete cycle of wave oscillation. The solitons propagate from right to left, the constant time interval between photographs is 20 s, and the average pycnocline thickness is $\bar{h} \simeq 2{\cdot}0$ cm. The effect of wave amplitude on the oscillation period is clear: the first half of the cycle from (*a*)–(*d*) occurs in approximately 60 s, while the remaining half-cycle from (*d*)–(*j*) takes approximately 120 s.

3. Results and discussion

A total of eleven experiments were performed, for which all requisite data were successfully obtained. The average time to stratify the tank, inject the kerosene–Freon droplets, run the interaction experiment, and measure the density profiles was approximately twelve hours. Generally only two interaction sequences were recorded for a given stratification set-up, because a continuous merging of the kerosene–Freon beads degraded the visual definition of the isopycnal surfaces to a point that precluded accurate wave-position and amplitude measurement. We only report data for wave interactions that occurred during the transit down the tank so as to exclude amplitude and phase variations resulting from the endwall collision.

In the presentation of data we adhere to the co-ordinate system and terminology defined in figure 3. The end wall is located 9·79 m from the co-ordinate origin at the end of the splitter plate. Data corresponding to upper and lower solitary waves will be represented by upward- and downward-pointing triangles respectively.

3.1. *Density profiles*

Sample ambient-density distributions are displayed in figures 5(*a*, *b*). The dotted lines are a linear least-squares fit to the data on the inner 50 % of the profiles used to define the maximum slope thicknesses $2h_i$ ($i = 1$, 2 corresponding to the upper and lower pycnoclines respectively) of each pycnocline. The solid circles represent the measured location of the kerosene–Freon droplets. As mentioned previously, the saline solutions were carefully set at $\rho_0 = 1{\cdot}05$ g/cm^3, $\rho_1 = 1{\cdot}02$ g/cm^3 and $\rho_2 = 1{\cdot}08$ g/cm^3. Thus the density jumps across each layer were nearly identical for all experiments: $|\rho_0 - \rho_i| \equiv 2\Delta\rho = 0{\cdot}030$ g/cm^3. Denoting $y = y_i$ as the centre of each pycnocline, the distributions in figure 4 can be approximated by the hyperbolic-tangent profiles

$$\rho = \rho_0 + \Delta\rho[1 \pm \tanh[(y - y_i)/h_i]], \tag{3.1}$$

in which upper and lower signs correspond to $i = 1$ and 2 respectively. A summary of the ambient-density-field parameters for each experiment is presented in the first five columns of table 1. Runs 1–3 each had a separate density calibration taken soon after completion of the experiment, and for the remaining run pairs (4, 5), (6, 7), (8, 9) and (10, 11) only a single calibration was taken between the two runs. A comparison of test profiles taken before and after an experiment yielded typically a 4 % increase in the maximum slope thickness caused by the redistribution of fluid from each mixed region into their respective pycnoclines. Hence the measured values of maximum slope thicknesses $2h_i$ for runs 1–3, 4, 6, 8, and 10 have all been multiplied by 0·96 to account for this growth.

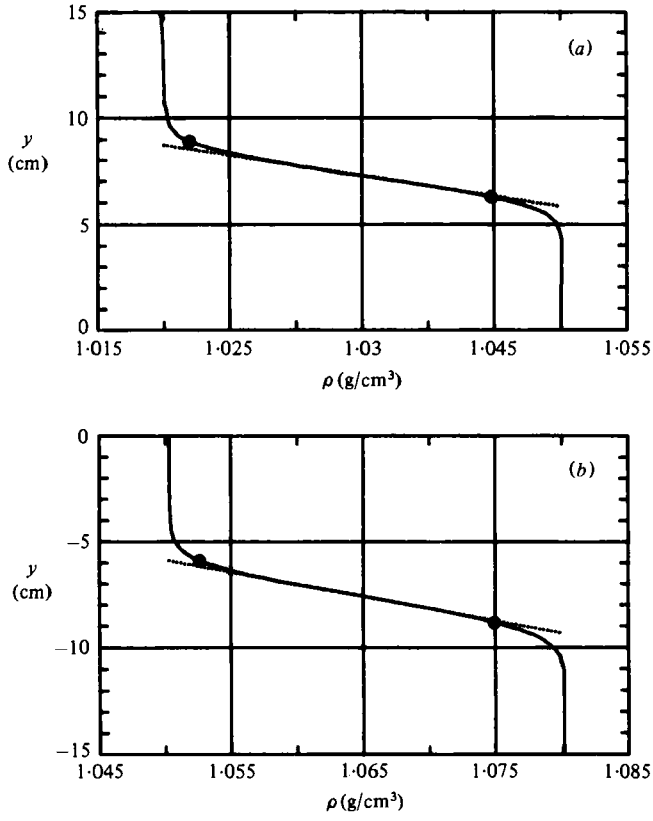

FIGURE 5. Measured density profiles for the upper (*a*) and lower (*b*) pycnoclines corresponding to run 2. The dotted line represents a fitted curve to the inner 50% of the profile defining the maximum slope, and the filled circles locate the positions of the kerosene–Freon droplets.

Run no.	H (cm)	D_1 (cm)	D_2 (cm)	$2h_1$ (cm)	$2h_2$ (cm)	C_{01} (cm/s)	C_{02} (cm/s)
1	15·26	7·92	7·20	4·41	4·54	3·37	3·36
2	14·89	7·72	7·76	2·80	3·48	2·84	3·07
3	15·13	8·04	7·19	2·82	3·48	2·86	3·07
4	15·25	8·04	7·09	4·01	4·16	3·28	3·26
5	15·25	8·04	7·09	4·18	4·34	3·36	3·31
6	15·16	7·99	7·17	3·62	4·20	3·15	3·28
7	15·16	7·99	7·17	3·78	4·38	3·20	3·32
8	15·22	7·98	7·10	4·31	4·79	3·36	3·41
9	15·22	7·98	7·10	4·49	4·99	3·40	3·45
10	14·79	7·71	7·82	2·61	2·94	2·77	2·90
11	14·79	7·71	7·82	2·72	3·06	2·81	2·95

TABLE 1. Environmental parameters and linear mode-two wave speeds

3.2. *Wave amplitudes and phase*

Amplitude measurements for run 1 corresponding to a relatively thick pycnocline experiment are presented in figure 6. The measured values for each wave a_1 and a_2 are seen in figure 6(*a*) to oscillate around some average, monotonically decreasing amplitude. This mean amplitude $\bar{a}$, approximated by a third-order least-squares Chebyshev-polynomial fit to the data normalized over the interval $[-1, 1]$, is shown by the dotted line. In an attempt to remove the effects of viscous dissipation we have calculated the difference amplitudes for the upper and lower waves

$$\Delta a_i = a_i - \bar{a} \quad (i = 1, 2), \tag{3.2}$$

and these are plotted in figure 6(*b*). Note that the attenuation of the peak amplitude of Δa_i is small compared with the attenuation of $\bar{a}$ for these relatively large-amplitude waves.

The individual (x_i, t) wave trajectories plotted in figure 6(*c*) show little hint of oscillation because the phase excursions are relatively small. The dotted line drawn through these measurements is a fourth-order Chebyshev-polynomial fit to the normalized data, and approximates the trajectory traced out by the system's centre of mass $\bar{x}$ travelling at the 'group' velocity C_g. The spatial phase of each wave relative to this centre of mass,

$$\Delta x_i = x_i - \bar{x} \quad (i = 1, 2), \tag{3.3}$$

is plotted versus time in figure 6(*d*) and exhibits nicely the spatial oscillations of the slowly varying solitons. Note that the phase excursions increase monotonically as the mean amplitude $\bar{a}$ decreases.

A comparison of certain features of the interaction with theoretical examples given by LKK and LPK is made with the aid of figures 7 and 8, which present evolution plots of Δa_i for two experiments along with their total phase defined as

$$\sigma = x_1 - x_2. \tag{3.4}$$

This comparison can only be considered qualitative for two main reasons. First, the characteristic non-dimensional amplitudes $\bar{a}_0/\bar{h}$, defined in § 3.4 and listed in table 3, are substantially greater than allowed by the weakly nonlinear theory. Secondly, if we denote the distance from a pycnocline to its nearest fluid boundary by D_i $(i = 1, 2)$ (see figure 3), then $D_1 = D_2 = H$ for the examples given in LKK and LPK, while the data reported here correspond to $D_1 \simeq D_2 \simeq \frac{1}{2}H$. (We do not anticipate that the free surface in our experiment used in lieu of the fixed upper boundary considered in the theoretical studies will yield qualitative differences in the flow fields, except in a small neighbourhood near the upper stress-free surface.)

The data in figures 7 and 8 correspond to relatively thick and thin pycnocline experiments, respectively. In comparing these results with figures 2(*c*, *d*) in LKK and figure 3 in the companion paper LPK, we note distinct similarities. First, although the peak-to-peak values are nearly equal, the difference amplitudes Δa_1 and Δa_2 do not vary about a common level. Also, both theory and experiment show that Δa_i and σ are approximately 90° out of phase. Furthermore, both the amplitude and period of the phase measurements in figures 7(*a*) and 8(*a*) are continuously increasing with time. This can be considered a direct consequence of the slowly decreasing amplitudes (cf. figure 6) of the solitons, in qualitative agreement with the theoretical trends predicted in LPK.

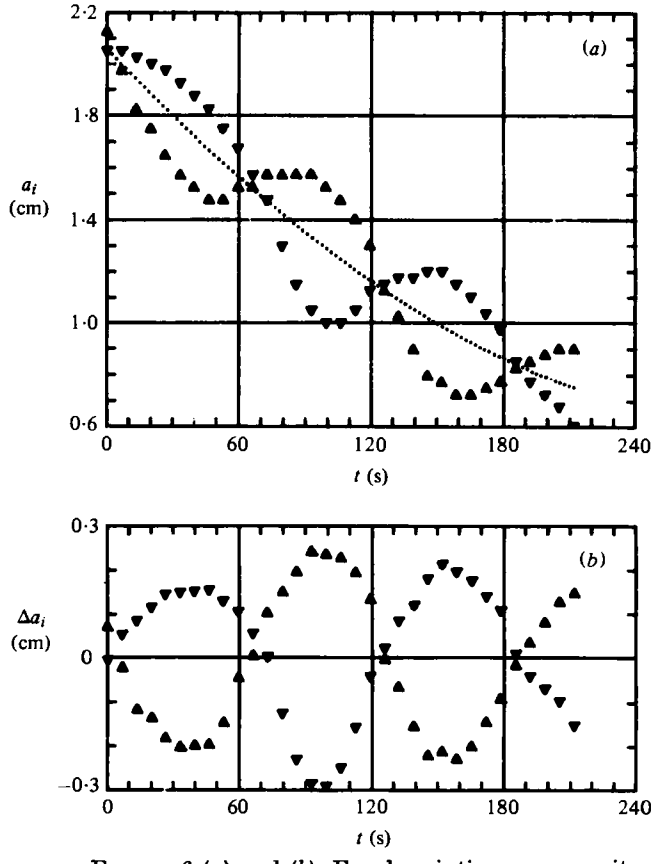

FIGURE 6 (*a*) and (*b*). For description see opposite.

3.3. *Wave speeds*

The numerical computations in LKK show that the nonlinear group velocity C_g of the wave system satisfies the inequality

$$\bar{C}_0 < C_g < \bar{C}, \tag{3.5}$$

where $\bar{C}_0$ and $\bar{C}$ are the average linear and nonlinear speeds of the interacting waves. Kubota, Ko & Dobbs (1978) have derived a general asymptotic expression for the linear long-wave phase speed of solitons propagating along single thin pycnoclines bounded above and below by rigid horizontal boundaries. Using their result for the hyperbolic-tangent profiles in (3.1), one obtains the following estimate for mode-two waves:

$$C_{0i} = \left[\frac{g\Delta\rho h_i}{2\rho_0}\right]^{\frac{1}{2}}\left[1 - \frac{3}{8}\left(\frac{h_i}{D_i} + \frac{h_i}{L_i}\right) + \ldots\right], \tag{3.6}$$

valid for h_i/D_i, $h_i/L_i \ll 1$, where $L_1 = H + D_2$ and $L_2 = H + D_1$. Thus in applying (3.6) we have assumed that the bounding walls for each soliton are the free surface and channel floor. The linear speeds calculated in this manner are listed in table 1. The fact that the upper boundary is really a free surface can have little effect on the linear wave speed since the speeds calculated for an upper free surface and for an upper

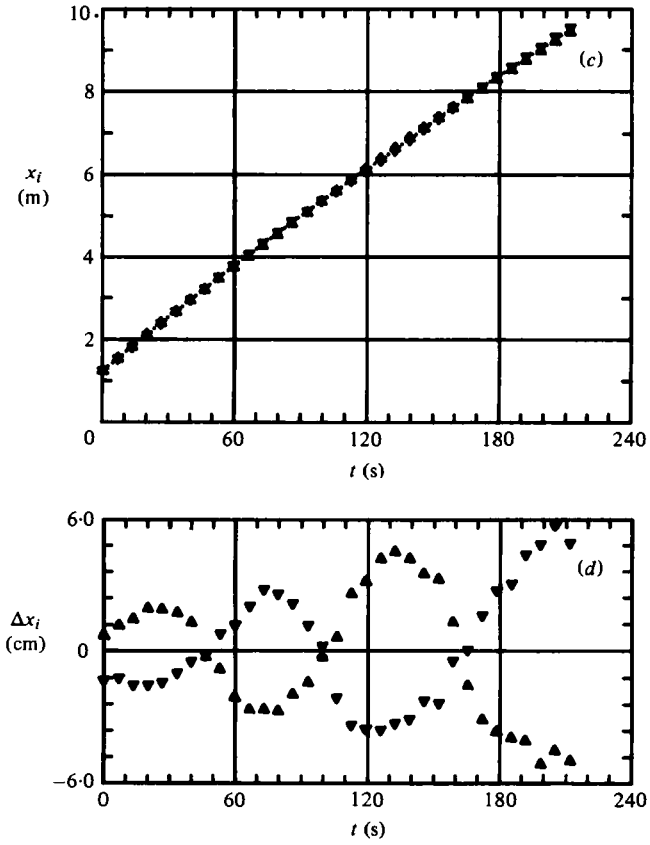

FIGURE 6. Measured interaction data corresponding to run 1. (*a*) Amplitude evolution of the upper (▲) and lower (▼) waves; the dotted line is a fitted curve representing the mean amplitude $\bar{a}$. (*b*) Evolution of the difference amplitudes. (*c*) Upper and lower wave trajectories; the dotted line is a fitted curve representing the wave centre $\bar{x}$. (*d*) Evolution of the phase of each soliton relative to the wave centre.

solid boundary differ only by an amount of order $(\Delta\rho/\rho_0)^{\frac{1}{2}}$. An alternative method of approximating the linear wave speeds, that of solving the eigenvalue problem for a broken-line density-profile model, has also been carried out. The results for runs 1–11 calculated in this manner are all within 4 % of those obtained using (3.6).

The group velocity $C_g = d\bar{x}/dt$ can be readily determined from the slope of the fitted curve $\bar{x}(t)$ describing the trajectory of the wave centre. A plot of the time evolution of C_g for run 1 corresponding to figure 6 is given in figure 9 (*a*). In figure 9 (*b*) the velocities are cross-plotted against the normalized amplitude $\bar{a}/\bar{h}$ at each corresponding time. These curves suggest that the group velocity does asymptote to $\bar{C}_0$ in the limit of zero wave amplitude, and the left-hand inequality in (3.5) is indeed satisfied. Further supporting evidence that the group speed always exceeds the average linear wave speed is given in table 2, which compares the calculated values of $\bar{C}_0$ with the terminal (smallest) value of C_g in each experiment. Having neglected to measure the nonlinear speed of single, non-interacting solitons, we are unable to test the right-hand inequality in (3.5).

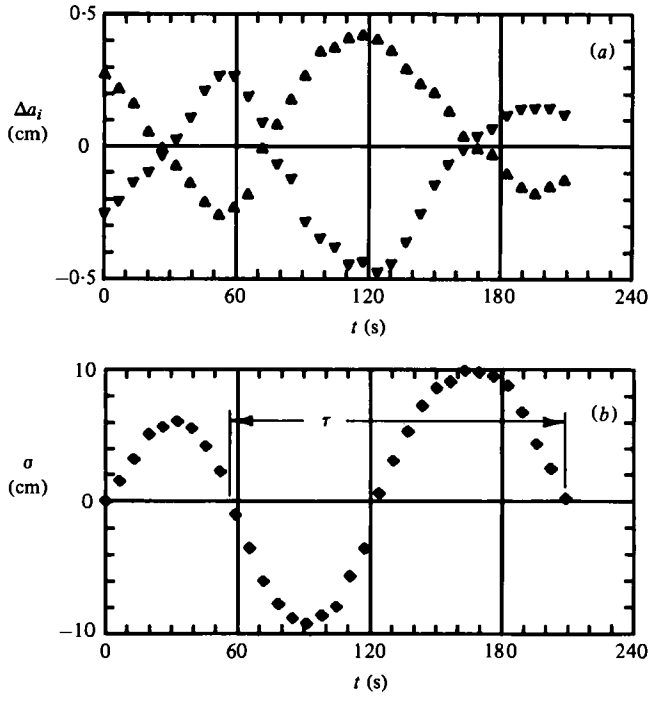

FIGURE 7. Evolution of (*a*) the difference amplitudes and (*b*) the total phase for run 8 corresponding to relatively thick pycnoclines. The data sequence used to determine the average period is indicated.

3.4. *Oscillation frequency*

Even in controlled fluid-dynamical experiments, a proper comparison of results with theoretical predictions for ideal fluid phenomena is often frustrated by unavoidable dissipation mechanisms. Strong-interaction experiments of the present kind are particularly susceptible to the action of viscosity because of the long timescales involved. Although the solitons may be considered quasisteady, their amplitude variations are not negligible during the time of leapfrog oscillation. Thus, in order to make a quantitative comparison with inviscid theoretical results, we take simple averages.

Average oscillation periods τ for each experiment were determined from the total phase plots. In choosing the range of data from which to obtain this average, the following criteria were observed.

(i) When two solitons evolved on a given pycnocline, only data for which the trailing soliton fell back permanently more than four wavelengths (to be defined) behind the oscillating pair was admitted.

(ii) Generally only *weak* soliton data were considered; in a couple of instances it was necessary to include *strong* soliton data, but these comprised just a few points at the beginning of a data sequence.

(iii) Only zero-crossings or peak-to-peak values were used to calculate the period of oscillation.

Criteria (i) and (ii) usually admitted only the downstream three-quarters of the data set, and criterion (iii) sometimes determined whether a full period (figure 7*b*) or only

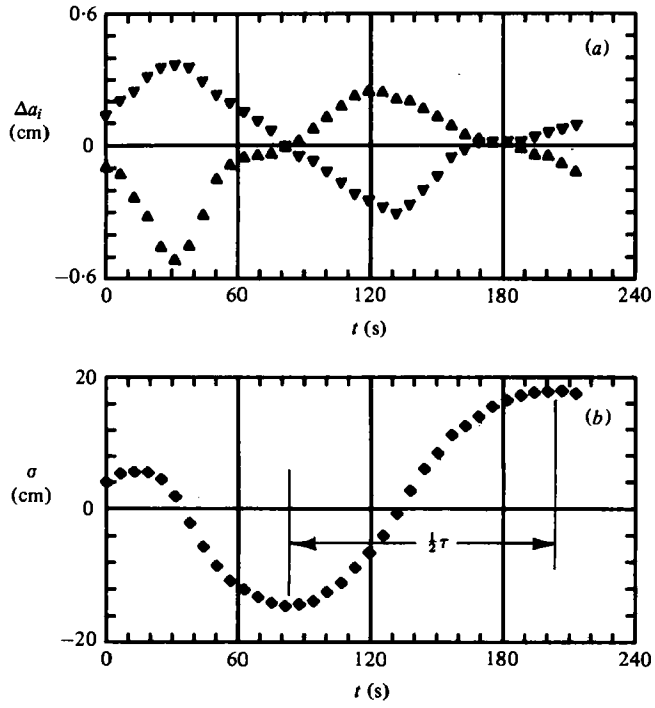

FIGURE 8. Evolution of (*a*) the difference amplitudes and (*b*) the total phase for run 11 corresponding to relatively thin pycnoclines. The data sequence used to determine the average period is indicated.

a half-period (figure 8*b*) of oscillation data was allowed. The median amplitude, denoted by $\bar{a}_0$, for the sequence of data considered was used to characterize the interaction, and is listed in non-dimensional form in table 3 along with the measured periods. Defining the wavelength λ as the soliton width at half-amplitude, we choose the characteristic wavelength $\bar{\lambda}_0$ to be the average of the upper and lower soliton wavelengths corresponding to $\bar{a}_0$. The measured values of LPK's separation parameter $\Delta = (\bar{\lambda}_0/H)^2$ are also listed in table 3.

Equation (18) of LPK for the oscillation frequency is strictly valid for Joseph solitons ($D_1 = D_2 = H$) that are weakly nonlinear ($\bar{a}_0/\bar{h} \ll 1$) and widely separated ($\Delta \ll 1$). In our experiment, although $D_1 \simeq D_2 \simeq \frac{1}{2}H$, we nevertheless anticipate that the increased separation distance will have only a weak influence on the soliton shape and speed. Thus, assuming the waves are characterized by Joseph solitons, we have used $\bar{a}_0$ and the environmental parameters given in table 1 to calculate the average Joseph wave-width parameter $\bar{\delta}_0 = \frac{1}{2}(\delta_{01} + \delta_{02})$ from equation (4*b*) of LPK by Newton iteration. These values, which necessarily lie in the interval $[0, \pi]$, are listed in table 3. In figure 10 we have plotted the experimental oscillation frequencies $\omega_{\text{exp}} = \tau/2\pi$ against the theoretical values ω_{th} calculated from equation (18) of LPK using the measured parameters listed in tables 1 and 3. Although the range of comparison is not large, we note reasonably good agreement in light of the sometimes $O(1)$ values of $\bar{a}_0/\bar{h}$ and Δ. We have omitted error bars because of the unknown effects of averaging and of assuming Joseph solitons. No apparent trend of the data with either the amplitude or separation parameters was discerned.

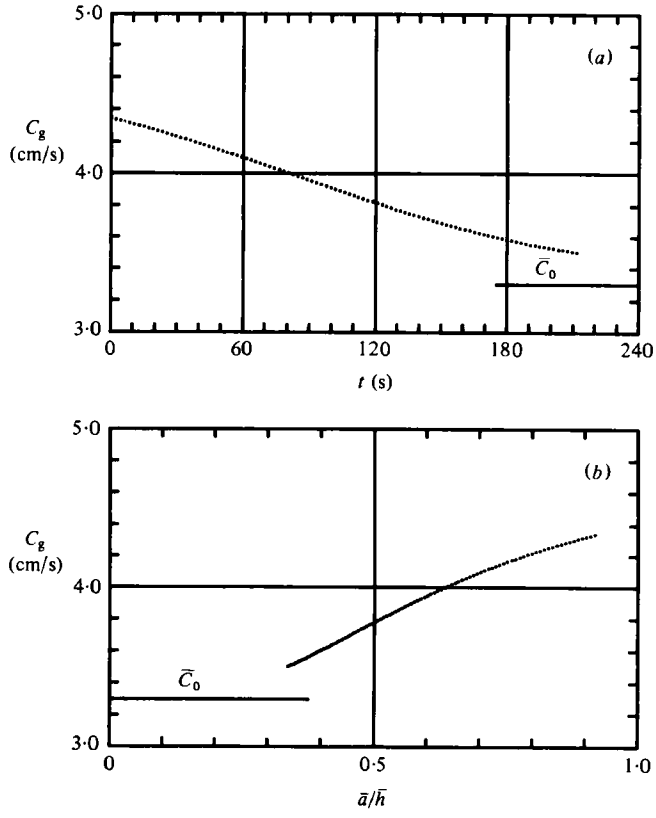

FIGURE 9. Group-velocity variation for run 1. (*a*) Group velocity as a function of time. (*b*) Group velocity plotted versus the non-dimensional mean wave amplitude.

Run no.	$\bar{C}_0$ (cm/s)	$(C_g)_{min}$ (cm/s)
1	3·37	3·50
2	2·97	3·20
3	2·97	3·08
4	3·27	3·27
5	3·33	3·39
6	3·22	3·30
7	3·26	3·46
8	3·38	3·42
9	3·43	3·53
10	2·83	3·29
11	2·88	3·43

TABLE 2. A comparison of the smallest measured group velocity $(C_g)_{min}$ and the average pycnocline wave speeds $\bar{C}_0$ calculated from (3.6)

Run no.	τ (s)	$\bar{a}_0/\bar{h}$	Δ	δ_0
1	130	0·47	0·47	1·88
2	140	0·65	0·35	2·28
3	180	0·61	0·53	2·25
4	196	0·39	0·39	1·82
5	220	0·48	0·45	1·93
6	198	0·58	0·58	2·09
7	168	0·58	0·46	2·06
8	176	0·38	0·60	1·74
9	129	0·51	1·07	1·90
10	240	0·83	0·16	2·47
11	200	1·02	0·35	2·55

TABLE 3. Measured periods and median non-dimensional amplitudes used to calculate the Joseph-soliton wave-width parameter δ_0. Also included are the measured estimates of the non-dimensional separation parameter $\Delta = (\bar{\lambda}_0/H)^2$.

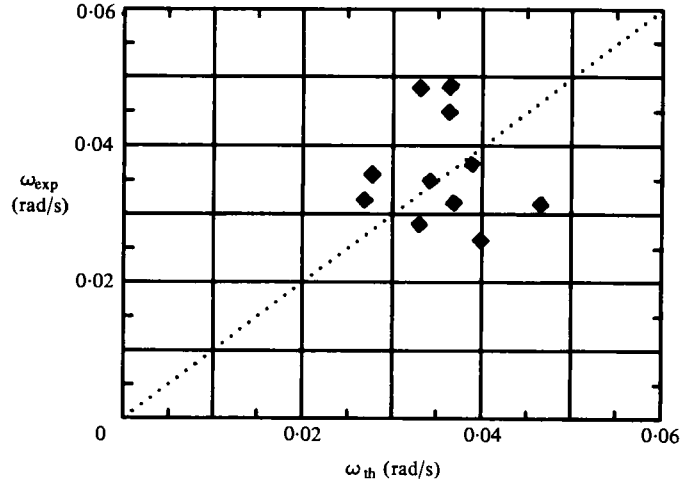

FIGURE 10. Oscillation-frequency measurements ω_{exp} compared with the theoretical prediction ω_{th} (equation (18) of LPK) computed from the parameters listed in tables 1 and 3.

In the limit $\Delta \to 0$, equation (18) of LPK reduces to the oscillation frequency for Benjamin–Davis–Ono (BDO) solitons,

$$\omega_{BDO} = \frac{3\pi^2(C_{01}^2 h_2^2 + C_{02}^2 h_1^2)^{\frac{1}{2}}}{8H^2}, \tag{3.7}$$

when $C_{01} \neq C_{02}$ (cf. equation (21) of LPK, for which $C_{01} = C_{02} = C_0$). A comparison of the measured frequencies with this asymptotic result computed from the parameters in table 1 is presented in figure 11. The disparity between theory and experiment in this figure gives a clear indication that the asymptotic limit was not obtained in the present experiment, as expected from the values of Δ listed in table 3.

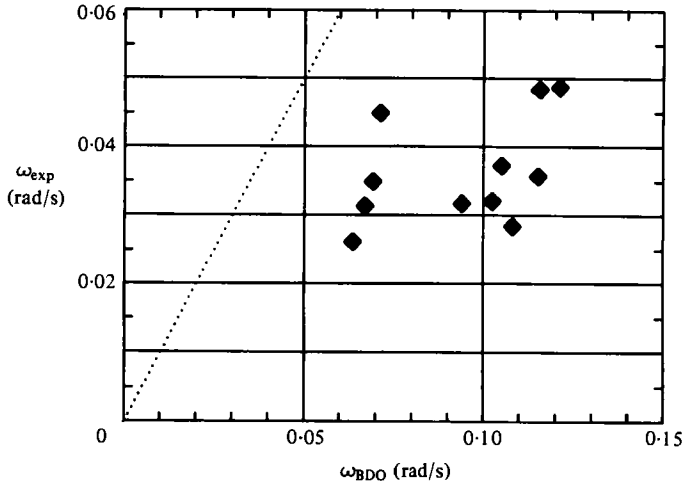

FIGURE 11. Oscillation-frequency measurements ω_{exp} compared with the asymptotic prediction ω_{BDO} (3.7) computed from the parameters listed in table 1.

3.5. *A three-soliton resonance*

In some cases two solitons ordered in amplitude evolved along each pycnocline from the mixed-region collapse. One such experiment resulted in a three-wave interaction between the two lead solitons and the nearest trailing soliton, the remaining soliton having been left behind. The difference amplitudes and phases for this interaction are presented in figure 12. Here the mean amplitude $\bar{a}$ and position $\bar{x}$ have been taken as the least-squares fit through the three amplitude and three trajectory curves respectively. In figure 12(*a*) the amplitudes are seen to decay more rapidly than in comparable two-wave interactions, and, again in comparison with similar two-wave interactions, a noticeably smaller group velocity was measured. Figure 12(*b*) shows that the leapfrog oscillation occurred between the two trailing solitons, while the upper lead soliton always remained in front. Figures 12(*a*, *b*) indicate that, while the lagging soliton on the upper pycnocline is 180° out of phase with its leapfrog partner, it is also nearly out of phase with the lead soliton. Unfortunately, we did not measure density profiles for this case, but estimates based on the kerosene–Freon droplet separation levels give $2h_1 = 2{\cdot}6$ cm and $2h_2 = 2{\cdot}8$ cm.

An explanation supporting the conjecture that the interaction might represent a three-soliton resonance is given with the aid of figure 13. The ideal waves are pictured travelling at the group velocity from left to right, with the initial configuration at the instant t_1 corresponding to zero time in figure 12. At time t_1 energy is cascaded backwards from the leading to the smaller trailing soliton on the upper layer, via the intermediate soliton on the lower layer. At time t_2 the upper rear soliton has grown in amplitude at the expense of the two forward waves, and proceeds to hop past the lower soliton. At time t_3 energy from the now large intermediate wave is transferred simultaneously upstream to the lead wave and downstream to the soliton on the lower pycnocline. The forward wave is then 'bumped' ahead via the Lax type (*a*) interaction, and at time t_4 the second hop between the trailing solitons is initiated. At time t_5 the solitons have returned to their approximate initial relative positions. In the actual

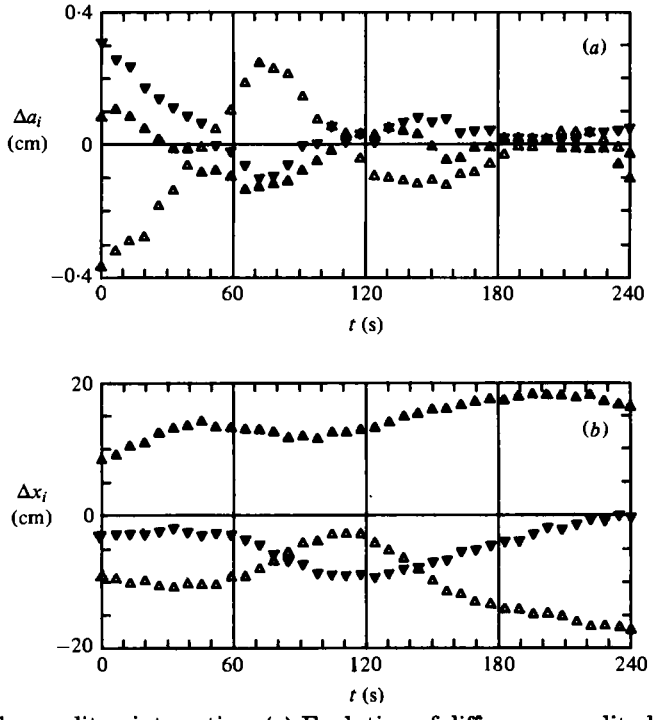

FIGURE 12. Three-soliton interaction. (*a*) Evolution of difference amplitudes for the first-upper (▲), first-lower (▼) and second-upper (△) solitons. (*b*) Evolution of the phase of each wave relative to the wave centre.

experiment the amplitudes decrease owing to viscous dissipation with a consequent increase in the horizontal excursions between the waves.

It appears that this is the first reported example of a soliton interaction that combines both *upstream* and *downstream* energy transfer. Our conjecture is that the ideal (inviscid) interaction is not a simple resonance, but may fall into the category of a Fermi–Pasta–Ulam (1955) recurrence phenomenon. The time-scale for forward energy transfer between solitons propagating along the same pycnocline is faster than the rearward energy transfer between solitons on neighbouring pycnoclines. This disparity in the energy-transfer timescales, becoming more pronounced with increasing pycnocline separation distance, probably precludes a simple hop–bump–hop repetition period. Other possibilities also exist, one of which is that the motion never repeats itself and hence is chaotic in the sense of strange-attractor dynamics.

4. Concluding remarks

In the foregoing experiments the evolving wave profiles were symmetric and slowly varying for sufficiently small wave amplitudes. Asymmetric profiles, probably a direct consequence of the mutually perturbed pressure fields set up by each soliton, were evident early in the interaction when the amplitudes were large. Our observations suggest that the distortion scales approximately with $\bar{a}/H$.

A curious irregularity was observed in runs 10 and 11, which represent the most

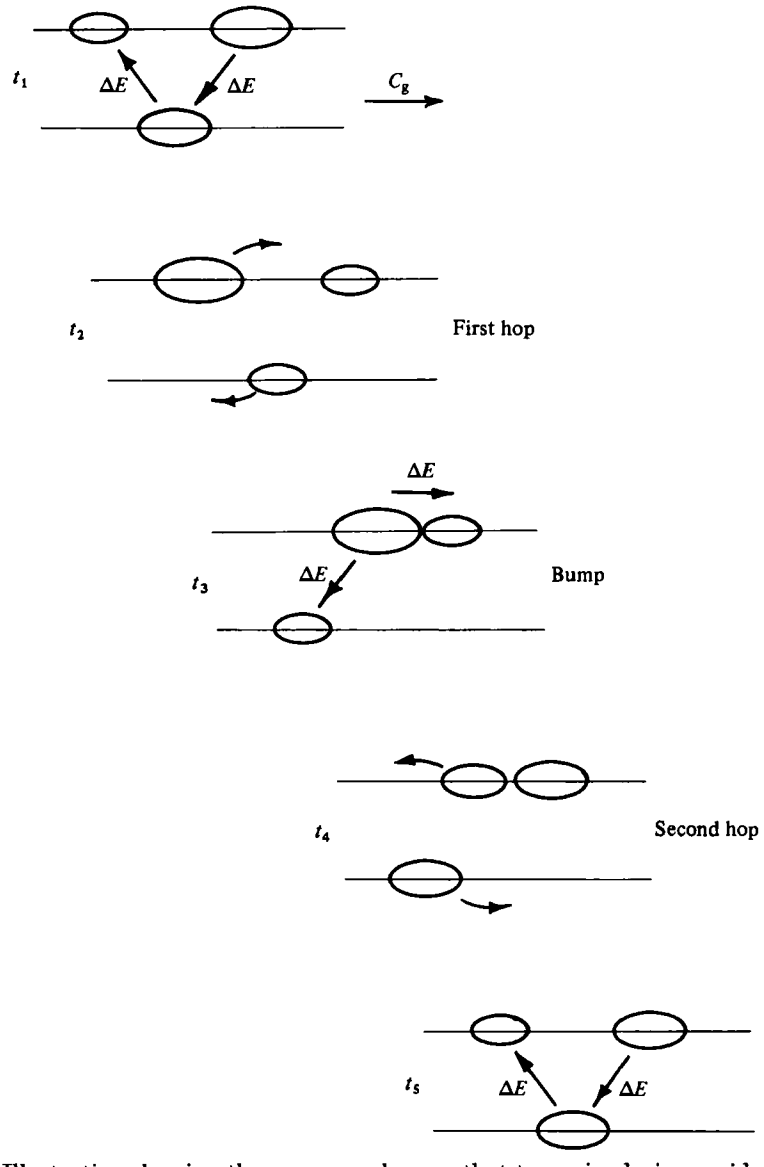

FIGURE 13. Illustration showing the energy exchanges that transpire during an idealized three-soliton interaction. The times $t_1, \ldots, t_5$ denote successive times during a complete cycle.

nonlinear ($\bar{a}_0/\bar{h} = O(1)$) interactions recorded. Here a flat spot in the difference amplitude curves (figure 8*a*) appeared when the waves were most widely separated. The occurrence of the plateau was repeatable, and seems to be purely a large-amplitude effect. The fact that this anomaly is not reflected in the phase measurements (figure 8*b*) can be explained by the fact that the phase σ is an integration (smoothing) of the amplitude, through the dependence of the nonlinear phase speed on soliton amplitude.

In conclusion, our experiments have demonstrated that two solitons propagating unidirectionally along neighbouring pycnoclines will oscillate in both amplitude and phase if their wave speeds are closely matched. Using simple averages and the assump-

tion that the waves can be described by Joseph solitons, we obtain reasonably good agreement with the predicted oscillation frequency reported in the LPK companion paper, even for relatively large-amplitude waves. A three-soliton resonance necessitating both forward and rearward energy transfer has also been observed and documented, perhaps for the first time. Although we suspect this interaction may represent a Fermi–Pasta–Ulam recurrence phenomenon, the exact nature of the resonance remains a subject for future study.

The authors wish to express their appreciation for the initial experimental efforts of Dan Raferty in developing a viable two-soliton wave generator. We are indebted to A. K. Liu, N. Pereira and L. Redekopp for discussions relating to theoretical aspects of the problem. The assistance of our laboratory technician Casey de Vries is always much appreciated. This work was supported by the Office of Naval Research under Grant no. N00014-76-C-0211.

REFERENCES

Amen, R. & Maxworthy, T. 1980 The gravitational collapse of a mixed region into a linearly stratified fluid. *J. Fluid Mech.* **96**, 65–80.

Eckart, C. 1961 Internal waves in the ocean. *Phys. Fluids* **4**, 791–799.

Fermi, E., Pasta, J. R. & Ulam, S. M. 1955 Studies of nonlinear problems. *Los Alamos Sci. Lab. Rep.* LA-1940.

Joseph, R. I. 1977 Solitary waves in a finite depth fluid. *J. Phys.* A*: Math. Gen.* **10**, L225–L226.

Koop, C. G. 1976 Instability and turbulence in a stratified shear layer. Doctoral thesis, Department of Aerospace Engineering, University of Southern California.

Kubota, T., Ko, D. R. S. & Dobbs, L. D. 1978 Weakly nonlinear, long, internal gravity waves in stratified fluids of finite depth. *J. Hydronautics* **12**, 157–165.

Lax, P. D. 1968 Integrals of nonlinear equations of evolution and solitary waves. *Commun. Pure Appl. Math.* **21**, 467–490.

Liu, A. K., Kubota, T. & Ko, D. R. S. 1980 Resonant transfer of energy between nonlinear waves in neighboring pycnoclines. *Stud. Appl. Math.* **63**, 25–45.

Liu, A. K., Pereira, N. R. & Ko, D. R. S. 1982 Weakly interacting internal solitary waves in neighbouring pycnoclines. *J. Fluid Mech.* **122**, 187–194.

Maxworthy, T. 1980 On the formation of nonlinear internal waves from the gravitational collapse of mixed regions in two and three dimensions. *J. Fluid Mech.* **96**, 47–64.

Weidman, P. D. & Maxworthy, T. 1978 Experiments on strong interactions between solitary waves. *J. Fluid Mech.* **85**, 417–431.